

Improving 68-Ga-PSMA PET/MR hybrid imaging of the prostate with un-renormalized absolute scatter correction

Maike E. Lindemann¹, Nika Guberina², Axel Wetter², Wolfgang Fendler³, Bjoern Jakoby⁴, Harald H. Quick^{1,5}

1 High-Field and Hybrid MR Imaging, University Hospital Essen, University Duisburg-Essen, Essen, Germany

2 Department of Diagnostic and Interventional Radiology and Neuroradiology, University Hospital Essen, University of Duisburg-Essen, Essen, Germany

3 Department of Nuclear Medicine, University Hospital Essen, University of Duisburg-Essen, Essen, Germany

4 Siemens MR, Siemens Healthcare GmbH, Erlangen, Germany

High-Field and Hybrid MR Imaging, University Hospital Essen, University Duisburg-Essen, Essen, Germany;

5 Erwin L. Hahn Institute for Magnetic Resonance Imaging, University Duisburg-Essen, Essen, Germany

Running title: Improved SC in prostate PET/MR

Word count: 4744

Corresponding first author:

Maike E. Lindemann, MSc

High-Field and Hybrid MR Imaging

University Hospital Essen

Hufelandstr. 55

D-45147 Essen, Germany

Electronic mail: maike.lindemann@uk-essen.de

Telephone: +492017232624

Fax: +492017231595

ABSTRACT

Purpose: A limitation of using 68-gallium-labelled prostate-specific membrane antigen (68-Ga-PSMA) for detection and staging of prostate cancer is a frequently observed halo artifact around the urinary bladder caused by inaccurate scatter correction (SC) of positron emission tomography (PET) data. The aim of this study is to investigate the impact of un-renormalized absolute SC on 68-Ga-PSMA PET quantification in PET/magnetic resonance (MR) hybrid imaging of the prostate in 100 patients.

Methods: The PET data of 100 patients were reconstructed twice using standard SC and improved un-renormalized SC. The visual presence of halo artifacts was rated in each PET data reconstruction using five grades (0 = no halo artifact, 4 = severe halo artifact). The number of visible lesions in the pelvis was recorded. Standardized-uptake-values (SUV_{mean} and SUV_{max}) were measured in the lesions, the bladder, in the gluteus maximus, and within the halo margin. Furthermore, the signal-to-noise-ratio (SNR) and image noise were measured in all PET data. Relative differences between standard and un-renormalized SC were calculated.

Results: With standard SC the average grade in halo presence was 2 (moderate halo-artifact), whereas for un-renormalized SC the average grade was 0.9 (slight halo-artifact). The same number of congruent lesions ($n=74$) was detected for both PET data reconstructions. Relative changes in PET signal-to-noise-ratio and image noise were statistically not significant ($p > 0.05$). The mean \pm standard deviation (SD) increase in SUV_{mean} in the gluteus maximus using un-renormalized SC was 23.0 ± 9.2 %, in the bladder 7.1 ± 4.5 %, in the halo-margin 325.4 ± 748.5 % and in all $n=74$ detected lesions 12.4 ± 16.8 %. The mean increase using un-renormalized SC in SUV_{mean} for lesions inside (38 lesions) the halo-margin was 17.5 % and outside (36 lesions) the halo-margin is 6.9 %.

Conclusions: For PET/MR hybrid imaging of prostate cancer using 68-Ga-PSMA a proper SC is important to ensure best possible diagnostic quality and PET quantification. The unrenormalized absolute SC significantly reduces the halo artifact around the bladder and improves PET/MR hybrid imaging of the prostate.

Key words: scatter correction; halo artifact; PET quantification; prostate PET/MR imaging; 68-Ga-PSMA

INTRODUCTION

Since the introduction of 68-gallium-labelled prostate-specific membrane antigen (68-Ga-PSMA) ligand as positron emission tomography (PET) tracer (1), several studies show promising results for the detection and staging of prostate cancer with PET/computer tomography (CT) (2-4) and, more recently, PET/magnetic resonance imaging (MRI) (5-9).

A potential challenge of using 68-Ga-PSMA for detection and staging of prostate cancer is a frequently observed photopenic artifact in PET images, known as “halo artifact”. PSMA barely accumulates in abdominal fat and soft tissue. The majority of 68-Ga-PSMA is excreted by the urine and thus concentrated within the urinary system. This results in extreme differences in activity concentration between the bladder/kidneys and surrounding background tissue and, thus, may lead to the halo artifact in PET/CT (10), but particular in PET/MR (5,8). The halo artifact causes reduced signal intensity around the urinary bladder and at the levels of the kidneys in scatter and attenuation corrected PET images (5,11,12) (Fig. 1). Due to this artificial PET signal extinction, tumor manifestations and lesions in these regions might be non-detectable by PET or may show distorted standardized-uptake-values (SUV) hampering quantification of lesion activity. In addition to the high specificity of PSMA, 68-Ga decay causes further physical challenges. In 68-Ga decay prompt gammas are emitted simultaneously with positron emission. These gammas have an energy of 1077 keV. When the gammas are scattered before detection, their energy might fall into the energy window of the PET system (e.g. 430-610 keV for Biograph mMR, Siemens Healthcare GmbH). A coincidence between prompt gammas and annihilation photons cannot be differentiated from true coincidences, and thus affect PET overall quantification and image quality.

The halo artifacts are often caused by inaccurate scatter correction (SC) (5,8,12). For this reason an optimized SC is needed to minimize the adverse effect of halo artifacts on diagnostic accuracy of prostate cancer in PET/MR imaging. The most common used SC method in clinical

PET imaging is based on the single scatter simulation algorithm (13,14). The absolute scaling of single scatter simulation for highly specific PET tracers such as 68-Ga-PSMA seems to be less prone to halo artifacts as the relative scaling (12). Heußer et al. (12) also demonstrated that a reduction of the maximum scatter fraction from 75 % to 40 % can suppress the halo artifact in 68-GA-PSMA prostate PET/MRI. An improved SC method for the Biograph mMR (Siemens Healthcare GmbH, Erlangen, Germany) uses un-renormalized absolute scatter correction. PET SC typically employs a single Compton scatter simulation to compute a scatter sinogram, which is scaled to the emission data to account for multiple and possible external scatter from outside of the scanner's field-of-view (FOV). Eliminating the sometimes problematic renormalizing (rescaling) of the PET emission image during the SC calculations for tracers like 68-Ga-PSMA can minimize the appearance of the halo artifact and therefore, improve diagnostic image quality and PET quantification.

Not correcting the prompt gammas may lead to a scatter overestimation when applying relative single scatter simulation (15). Therefore, a prompt gamma correction might be beneficial in some cases combined with relative single scatter simulation showed by Heußer et al. (12). Especially in PET/CT imaging the prompt gamma correction seems to reduce halo artifacts around the kidneys (16). Nevertheless, Noto et al. (9) and Heußer et al. (12) both revealed that prompt gammas had a limited effect on the appearance of halo artifacts in 68-Ga-PSMA PET/MR imaging. Potential reasons for why prompt gamma correction is more effective in PET/CT as PET/MR might be the arm posing (arms up in PET/CT, arms down in PET/MR) and the often longer post injection times in PET/MR (often patients first underwent a PET/CT and subsequently a PET/MR examination without further tracer injection). A prompt gamma correction has been shown to inherently improve PET quantification using isotopes such as 82-Rubidium with a much higher branching fraction than 68-Ga (15). However, the prompt gamma branching fraction for 68-Ga is 3 %, and only a fraction of these will be detected in coincidence

with the annihilation radiation. In other words, the prompt gamma background is very low and doesn't have a significant impact on the absolute scatter.

While prompt gamma correction seems to have negligible impact on 68-Ga-PSMA PET/MR imaging and the appearance of halo artifacts (9,12) new multi-scatter methods show promising results (17). Yet under development, the double scatter simulation in addition to single scatter simulation seems to be a good approximation to the total scatter, and therefore might further improve 68-Ga-PSMA PET/MR imaging.

Due to the high interest in 68-Ga-PSMA PET for staging, therapy and follow-up of prostate cancer (18-20), the frequent occurrence of halo artifact in conjunction with this radiotracer presents a challenge for diagnostic image interpretation. To improve clinical diagnostic and scientific evaluation of 68-Ga-PSMA PET/MR and also PET/CT imaging, a robust SC method is needed to reduce the halo artifact. The aim of this study was to investigate the qualitative and quantitative impact of un-renormalized absolute SC on 68-Ga-PSMA PET quantification in PET/MR hybrid imaging of the prostate in 100 patients.

MATERIALS AND METHODS

Patient Population

In this retrospective study 100 patients, who underwent a pelvic 68-Ga-PSMA PET/MR examination, were included. The patient population (mean age 69.3 ± 7.8 years, interquartile range 12.6 years; mean body-mass-index 27.1 ± 3.5 kg/m², interquartile range 4.0 kg/m²) were administered an average radiotracer dosage of 117.2 ± 29.7 MBq (interquartile range 52.3 MBq). The PET/MR measurement started 138 ± 69 minutes post injection (interquartile range 111 min). Patients received 20 mg Furosemide 15 minutes post injection. Patients were referred to pelvic 68-Ga-PSMA PET/MR either because of suspected primary prostate carcinoma or biochemical recurrence. The institutional review board (Ethics Commission of the Medical Faculty of the University Duisburg-Essen) approved this study (study number 11–4822-BO) and all subjects signed a written informed consent.

Image Acquisition and Reconstruction

PET/MR measurements were performed on an integrated 3-Tesla whole-body PET/MR system (Biograph mMR, Siemens Healthcare GmbH, Erlangen, Germany). All patients were asked to void their bladder directly before PET acquisition. PET data of the pelvis were acquired for 10 to 40 minutes, followed by a whole-body PET examination (3-5 bed positions, 4 min/bed position). Arms were positioned along the body. Latest methods for MR-based attenuation correction (AC), respectively a standard Dixon-VIBE (volumetric interpolated breath-hold examination) sequence supplemented with MR-based HUGE (B₀ Homogenization Using Gradient Enhancement) information from extended FOV (21) and segmented bone information, were used as a basis for attenuation and scatter correction (22). All PET data reconstruction was performed with e7 tools (Siemens Molecular Imaging, Knoxville, USA) using OP-OSEM (ordinary

Poisson ordered-subsets expectation maximization) algorithm with 3 iterations, 21 subsets and 4 mm Gaussian filter. Random, scatter and decay correction was applied for all PET emission data. For comparability reasons, for each patient a 10 minute time interval from the start of the PET measurement was obtained from the list-mode data in pelvis only. To validate the impact of SC on 68-Ga-PSMA PET/MR imaging, all PET data (pelvis only) from all 100 patients were reconstructed twice using standard SC (software version VE11 SP1) serving as the reference standard and un-renormalized SC (software version VE11 SP2). The vendor-based implementation of the single scatter simulation algorithm was used for scatter estimation with an absolute scaling of the estimated scatter. Both methods of SC, standard and un-renormalized, based on absolute single scatter simulation. The un-renormalized version of SC just omits the last scaling step. Default parameters were used and kept constant for all reconstructions (number of iterations 2, maximum scatter fraction 75 %, scale factor 1.0). To evaluate the potential impact of PET acquisition time on PET image quality and lesion detection, for a subset of two patients with lesions inside the halo margin, a 4-minute time interval from the start of the PET measurement was obtained from the list-mode data in the pelvis and compared to the standard 10-minute time intervals.. As for the 10-minute PET data, the 4-minute PET data was reconstructed with both SC methods (SP1 and SP2).

Image Analysis

The margins of the halo artifacts were mostly inhomogeneous and, thus, the accurate measurement of the halo volume were not feasible (5). Therefore, the presence and visibility of the halo was rated in 5 grades as follows: 0 = no halo artifact, 1 = slight halo presence, 2 = moderate halo presence, 3 = strong halo presence, and 4 = severe halo. For quantitative evaluation of PET image quality, standardized uptake values (SUVs), respectively SUV_{mean} , SUV_{max} and SUV_{SD} , were measured in the bladder, in the halo margin and the gluteus maximus.

All PET/MR data sets were analyzed regarding lesion detectability, applying a lesion detectability score (9). The 4-point detectability score was defined as 0 = not detectable, 1 = equivocal, 2 = discernible, and 3 = clearly visible. To quantify lesion detectability, SUV_{mean} , SUV_{max} and SUV_{SD} were obtained in all recorded lesions in each patient and for each of the two PET data reconstructions. All region-of-interest and volume-of-interest were copied in identical planes and positions in each reconstructed data set for each patient. Relative differences between standard and improved SC were calculated. Signal-to-noise (SNR), image noise and orbit-to-background-ratio (OBR) were generated. For statistical analysis the IBM SPSS version 22 software (SPSS Inc, Armonk, NY, USA) was used. Statistical analysis (t-test, X^2 test) was performed to compare the two SC methods, p-values < 0.05 were considered to be statistically significant.

RESULTS

Table 1 shows the presence of halo artifact rating in grades for 100 patients. With standard SC the mean grade was 2 (moderate halo artifact), whereas for un-renormalized SC the mean grade was reduced to 0.9 (slight halo artifact). With standard SC only in one patient data set no halo artifact (grade 0) was detected, while in three PET data sets a severe halo (grade 4) was visible. With un-renormalized SC in 23 patients no halo-artifact (grade 0) was visible and no PET data set presented with a severe halo (grade 4). The calculated p-value from a χ^2 test is less than 0.01, and therefore the grade of halo presence is dependent on the used SC method.

In all 100 patients, the same number of congruent lesions (n=74) was detected for both PET data reconstructions. Thus, no lesion was completely missed-out due to halo artifacts, independent of the SC method used. The lesion detectability score showed no differences between standard and un-renormalized SC. The lesions were rated with 2.5 ± 0.6 (discernible to clear visible) the same in both reconstructions, regardless of the halo artifacts.

The calculated p-values from the t-test were used to clarify if the changes in different parameters between standard and un-renormalized SC are statistically significant. The Bland-Altman plots in Figure 2 show the relative difference in measured SUV_{mean} and SUV_{max} in the gluteus maximus, the bladder, the halo margin and in all detected lesions using standard and un-renormalized SC. Note the overall gain in SUV values (SUV_{mean} and SUV_{max}) due to un-renormalized SC. A remarkable gain in SUV was measured within the halo margin. Considering all 100 patients, the mean \pm standard deviation (SD) increase in SUV_{mean} in the gluteus maximus using un-renormalized SC was 23.0 ± 9.2 % when compared to the standard SC (SP1). The total range for SUV_{mean} was 9.9 % up to 75.7 %. The mean \pm SD increase in SUV_{max} in the gluteus maximus using un-renormalized SC was 15.8 ± 7.9 %. The total range was 0.2 % up to 50.9 %. The changes in SUV_{mean} and SUV_{max} in the gluteus maximus are both statistically

significant ($p < 0.05$). The mean \pm SD increase over 100 patients in SUV_{mean} in the bladder using un-renormalized SC was 7.1 ± 4.5 % when compared to SP1. The total range was 0 % up to 16.7 %. The mean \pm SD increase in SUV_{max} in the bladder using un-renormalized SC was 5.9 ± 3.8 %. The total range was 0.1 % up to 14.7 %. The changes in SUV_{mean} and SUV_{max} in the bladder are both statistically significant ($p < 0.05$). Considering all 100 patients, the mean \pm SD increase in SUV_{mean} within the halo margin using SP2 was 325.4 ± 748.5 % when compared to SP1, the median was 127.3 %. The total range was 35.5 % up to 5463.4 %. The mean \pm SD increase in SUV_{max} in the halo margin using SP2 was 163.0 ± 250.5 %, the median was 77.3 %. The total range was 12.6 % up to 1327.4 %. The changes in SUV_{mean} and SUV_{max} in the halo margin are both statistically highly significant ($p < 0.01$). Considering all 74 detected lesions, the mean \pm SD increase in SUV_{mean} using un-renormalized SC was 12.4 ± 16.8 % when compared to the standard SC (SP1), the median was 7.4 %. The total range was -6.3 % up to 105.6 %. The mean \pm SD increase in SUV_{max} in all detected ($n=74$) lesions using un-renormalized SC was 5.5 ± 6.1 %. The total range was -1.7 % up to 33.8 %. The changes in SUV_{mean} and SUV_{max} in the lesions are statistically significant ($p < 0.05$).

Figure 3 shows boxplots of the OBR, image noise and SNR in the gluteus maximus, the bladder, the halo margin and the detected lesions using standard SC in comparison to un-renormalized SC. Note that the OBR and image noise decrease with un-renormalized SC, while SNR slightly increases. The mean \pm SD OBR decreased from 434.0 ± 698.3 using SP1 to 137.9 ± 182.3 when using SP2. The median OBR decreased from 171.6 to 82.6 with un-renormalized SC. The changes in OBR are statistically highly significant ($p < 0.01$). The mean \pm SD image noise also decreased with un-renormalized SC from 46.6 ± 22.9 % to 43.1 ± 20.2 %. The mean \pm SD SNR in the gluteus maximus increased with un-renormalized SC from 2.6 ± 1.1 to 2.8 ± 1.2 . The mean \pm SD SNR in the bladder increased with un-renormalized SC from 9.6 ± 3.9 to 10.2 ± 4.1 . The mean \pm SD SNR in the halo margin increased with un-renormalized SC from 1.8 ± 0.8 to 2.3 ± 0.8 . The mean \pm SD SNR in the lesions increased with

un-renormalized SC from 2.0 ± 0.9 to 2.4 ± 1.7 . The changes in image noise and SNR in each region are not significant ($p > 0.05$).

Relative differences in SUV_{mean} and SUV_{max} between standard and un-renormalized SC were calculated. All detected ($n=74$) lesions were divided into lesions detected inside (38 lesions) or outside (36 lesions) the halo margin. The mean \pm SD increase using un-renormalized SC in SUV_{mean} for lesions inside the halo-margin was 17.5 ± 20.5 % and outside the halo margin 6.9 ± 8.7 %, in SUV_{max} for lesions inside the halo margin was 7.4 ± 7.4 % and outside 3.5 ± 3.1 %.

Figure 4 shows a patient example with relative difference maps, with PET data corrected with SP1 and SP2, and MR data as well as fused PET/MR images. Three lesions could be detected in the SP1, respectively SP2 reconstructed PET data. Halo artifact in this example was reduced from severe halo presence (grade 4) to no halo artifact (grade 0) using SP2. Relative differences in SUV_{mean} of 47.4 % (lesion at ischium right), 32.0 % (lesion at pubis right) and 50.0 % (lesion at pubis left) in the lesions were calculated.

Figure 5 shows a patient example with relative difference maps, with PET data corrected with SP1 and SP2, and MR data as well as fused PET/MR images. One lesion inside the halo margin could be detected in the SP1, respectively SP2 reconstructed PET data. Halo artifact in this example was reduced from strong halo presence (grade 3) to no halo-artifact (grade 0) using SP2. A relative difference in SUV_{mean} of 105.6 % in the lesion was calculated.

Figure 6 shows axial PET images of two patient examples for a 10 and 4 minute time interval corrected with SP1 and SP2. In both time intervals for both patients the halo artifact could be reduced with un-renormalized SC. All lesions in all patients could be detected in all reconstructions. Comparing the visibility of one lesion in each patient (marked with red arrows) in the 4-minute time interval for standard and un-renormalized SC, the lesion is more faint in the

PET image with standard SC. The visibility score in these two examples decreased with standard SC compared to un-renormalized SC from discernible to equivocal in patient example 1 and from clear visible to discernible in patient example 2.

DISCUSSION

Inaccurate SC is a significant factor in the origin and extent of halo artifacts (5,12). By turning off the SC the halo could be virtually omitted. However, assessing non-scatter corrected PET images runs the risk of missing prostate cancer lesions and no quantification of the uptake values is possible. Another strategy to reduce the halo artifact is voiding the bladder prior to PET acquisition. Both strategies did not show a relevant effect on presence of the halo artifact (11). To ensure best possible diagnostic quality and PET quantification in PET/MR, an improved SC is needed. In this study the latest SC method for the Biograph mMR (Siemens Healthcare GmbH, Erlangen, Germany) PET/MR system using un-renormalized absolute SC is used to evaluate the improved effect of un-renormalized absolute SC on halo artifacts in 100 68-Ga-PSMA patients with prostate cancer.

SC algorithms in PET/MR hybrid imaging rely on an accurate AC-map of the patient tissues. Especially the frequently occurring truncations along the arms in the AC-map due to a limited MR FOV seem to be an important factor on the occurrence of halo artifacts (9,11). Inaccurate AC due to a limited MR FOV and therefore, truncation along patients' arms in the AC-map, lead to increased appearance of halo artifact (9,11). State of the art of AC in PET/MR hybrid imaging is a segmentation approach based on a Dixon-VIBE MR sequence, which divides the MR image into four tissue classes (background air, lung, fat and soft tissue) and assigns predefined linear attenuation coefficients to the segmented tissue regions (23). Latest methods of AC extend the standard Dixon AC-map including a bone model approach (24,25) and a MR-based FOV extension method called HUGE, which optimizes the readout gradient to locally compensate the B_0 inhomogeneities, and thus the truncations along the arms in the standard

Dixon-VIBE AC-map (21,26,27). In this study the latest MR-based AC method was used for both PET data reconstructions, standard and un-renormalized absolute SC, to further reduce the halo artifact.

Using the un-renormalized absolute SC inherently reduces the presence of halo artifacts from moderate-strong (grade 2-3) to slight-no (grade 0-1) halo presence. Average SUVs within the halo margin increase around 325 %, and therefore, considerably affect the quantitative assessment of prostate cancer in PET/MR hybrid imaging. Especially lesions inside the halo margin benefit from un-renormalized absolute SC, average relative differences of 17.5 % were calculated. In this patient cohort all congruent lesions could be detected in both reconstructions (standard vs. improved SC) with equivalent visibility ratings. Thus, no lesion was completely missed-out due to halo artifacts, independent of the SC method used. The average SNR and image noise was not affected by un-renormalized absolute SC.

The main limitation of this study is that although the improved effects of absolute scaling and un-renormalized SC indeed inherently reduce the presence of halo artifacts and improved overall PET image quality, this had no effect on lesion detection in this study population. This is a retrospective study including 100 patients, who underwent a pelvic 68-Ga-PSMA PET/MR examination. Because of the retrospective study design, post injection tracer accumulation times show a larger variation (138 ± 69 minutes post injection) across the included study population. Ideally, the post injection time should be less variant within the study population. Choosing only patients with confirmed (e.g. by biopsy) prostate carcinoma like in other studies (8,11,12) potentially could have increased the overall number of detected lesions and case studies. This may have provided better clinical assessment of the effect of absolute un-renormalized SC on lesion detection and quantification. Additionally, the lesions detected in this study may not have been on the detection threshold (not small or faint enough or near enough to the bladder) to be affected by the halo artifact. Nevertheless, the benefit in image quality and PET quantification

due to absolute un-renormalized SC on 68-Ga-PSMA PET/MR is evident. This is an important precondition to ensure best possible clinical assessment and diagnostic quality and to increase diagnostic confidence in 68-Ga-PSMA prostate PET/MR.

One aspect with potential impact on lesion detection is the duration of the PET data acquisition window. In contrast to previous studies (9,10,12), where the occurrence and extend of the halo artifact have been linked to impaired lesion detection, in the present study all lesions could be detected in all reconstructions, with or without halo artifact present. In this context, different PET acquisition time intervals and associated count statistics may have an impact on lesion detection. PET acquisition time in the previous studies was 4 minutes per bed position. Whereas, in the present study the PET data of the pelvis were acquired for 10 minutes or even longer. The prolonged MR protocol consisting of multiple sequences (e.g. T1, T2, diffusion weighted imaging) to generate a choice of soft tissue contrasts allowed for extended PET data acquisition in this study. The longer PET acquisition times and associated improved count statistics in the present study may have supported the detection of all lesions, even small or faint ones, in the pelvis despite the presence of halo artifacts.

Figure 6 illustrates the potential dependency of lesion visibility on PET acquisition time. In the 10-minute time interval all lesions are visible equally despite the halo artifact around the bladder. As for the 10-minute time interval PET image quality and lesion visibility increases in the 4-minute interval when using un-renormalized SC compared to standard SC for PET image reconstruction. However, the 4-minute time interval shows inherently reduced count statistics as to be expected. The overall visibility of the lesions is decreased when compared to the 10-minute time interval and especially when applying only standard SC. Detection of faint lesions within the halo artifact margin may be limited when using short PET acquisition times in combination with non-optimized scatter correction.

The proposed SC in this study inherently reduces the halo artifact, independent of the PET acquisition time. This is an important aspect for optimized and shorter 68-Ga-PSMA

PET/MR imaging protocols aiming at improved patient comfort and throughput. Such a short 68-Ga-PSMA PET/MR imaging protocol with 4 minutes PET acquisition time per bed position is now implemented on the Biograph mMR PET/MR system and the un-renormalized absolute SC will also be tested in this scenario in further studies to ensure best possible lesion detectability with reduced halo artifact.

The interest in 68-Ga-PSMA PET for staging, therapy and follow-up of prostate cancer is high (18-20), but the frequent occurrence halo artifact presents a challenge. In former 68-Ga-PSMA PET/MR studies lesions were missed-out due to the presence of halo artifacts (8,9,11,12). Therefore, an improved SC and reduction of the halo artifact is essential and represents a precondition to ensure best possible image quality and clinical assessment in prostate PET/MR. Quantitative 68-Ga-PSMA PET including SUV measurements is not yet fully established for clinical lesion quantification and treatment response assessment. However, the PET signal correlates with the absolute PSMA expression level. Several groups have recently proposed standardized interpretation criteria and lesion follow-up, thus reliable SUV measurements may become critical part of future interpretation systems and clinical assessment (28-30). The reduction or even elimination of halo artifacts is an important precondition for accurate quantification and standardization in this context.

The potential of 68-Ga-PSMA PET/MR hybrid imaging of the pelvis and abdomen was demonstrated in several studies (5-7) combining the excellent diagnostic performance of 68-Ga-PSMA PET for e.g. lymph node metastases and the soft tissue contrast and high spatial resolution of MRI without further radiation exposure compared to PET/CT. Nevertheless, PET/CT is still referred to as the gold standard (5,7). Halo artifacts may occur in both hybrid modalities, but particularly in PET/MR which is mostly related to the method of how SC is performed. The improved SC version with un-renormalized absolute scaling could inherently

reduce the halo artifact in this PET/MR study. Applying SC with un-renormalized absolute scaling may be also relevant for PET/CT imaging to further reduce the halo artifact.

While high uptakes in lesions usually are detectable even with a halo artifact present (results of this study), faint uptake in pathological structures may be masked by the halo artifact (8,11,12). To avoid false-negative diagnosis and a bias in PET quantification, artefact-free PET images are mandatory independent of the clinical workflow (e.g. sufficient patient hydration, tracer accumulation times). To ensure the visualization of all present lesions, we recommend a careful analysis of both PET images, scatter corrected and non-corrected. The vendor-based implementation of the single scatter simulation algorithm with absolute scaling and un-renormalized estimated scatter is a robust SC method relevant for 68-Ga-PSMA PET/MR and PET/CT imaging. Further improvements are to be expected with multiple-scatter methods, which are currently under development (17). This will help to improve scientific evaluation and clinical assessment.

CONCLUSION

For quantitative PET/MR hybrid imaging of prostate cancer using 68-Ga-PSMA a proper SC is important to ensure best possible diagnostic quality and PET quantification. The unrenormalized absolute SC significantly reduces the halo artifact around the bladder, and therefore improves PET/MR hybrid imaging of the prostate. SUVs in the halo margin increase averaged around threefold, and therefore, considerably affect the quantitative assessment of prostate cancer in PET/MR hybrid imaging.

DISCLOSURE

The current implementation of the scatter correction was provided by Siemens Healthcare GmbH, Erlangen, Germany. This work was supported by a research agreement between the University Hospital Essen and Siemens Healthcare GmbH, Erlangen, Germany. Bjoern Jacoby, PhD, is an employee of Siemens Healthcare, Erlangen, Germany. No other potential conflicts of interest relevant to this article exist.

KEY POINTS

Question:

Study purpose is to investigate the impact of un-renormalized absolute scatter correction on 68-Ga-PSMA PET image quality and quantification in PET/MR hybrid imaging of the prostate in 100 patients.

Pertinent findings:

The un-renormalized absolute scatter correction significantly reduces frequently observed halo artifacts around the bladder thus improving PET image quality and PET quantification in 68-Ga-PSMA PET/MR hybrid imaging of the prostate.

Implications for patient care:

Latest scatter correction methods in PET/MR help to improve diagnostic evaluation of prostate cancer in otherwise frequently artifact-hampered pelvic regions.

REFERENCES

1. Afshar-Oromieh A, Haberkorn U, Eder M, Eisenhut M, Zechmann CM. [68Ga]Gallium-labelled PSMA ligand as superior PET tracer for the diagnosis of prostate cancer: comparison with 18F-FECH. *Eur J Nucl Med Mol Imaging*. 2012;39:1085-1086.
2. Afshar-Oromieh A, Avtzi E, Giesel FL, et al. The diagnostic value of PET/CT imaging with the (68)Ga-labelled PSMA ligand HBED-CC in the diagnosis of recurrent prostate cancer. *Eur J Nucl Med Mol Imaging*. 2015;42:197-209.
3. Eiber M, Maurer T, Souvatzoglou M, et al. Evaluation of hybrid ⁶⁸Ga-PSMA ligand PET/CT in 248 patients with biochemical recurrence after radical prostatectomy. *J Nucl Med*. 2015;56:668-674.
4. Schwenck J, Rempp H, Reischl G, et al. Comparison of 68Ga-labelled PSMA-11 and 11C-choline in the detection of prostate cancer metastases by PET/CT. *Eur J Nucl Med Mol Imaging*. 2017;44:92-101.
5. Afshar-Oromieh A, Haberkorn U, Schlemmer HP, et al. Comparison of PET/CT and PET/MRI hybrid systems using a 68Ga-labelled PSMA ligand for the diagnosis of recurrent prostate cancer: initial experience. *Eur J Nucl Med Mol Imaging*. 2014;41:887-897.
6. Eiber M, Nekolla SG, Maurer T, Weirich G, Wester HJ, Schwaiger M. (68)Ga-PSMA PET/MR with multimodality image analysis for primary prostate cancer. *Abdom Imaging*. 2015;40:1769-1771.
7. Freitag MT, Radtke JP, Hadaschik BA, et al. Comparison of hybrid (68)Ga-PSMA PET/MRI and (68)Ga-PSMA PET/CT in the evaluation of lymph node and bone metastases of prostate cancer. *Eur J Nucl Med Mol Imaging*. 2016;43:70-83.
8. Lütje S, Blex S, Gomez B, et al. Optimization of acquisition time of 68Ga-PSMA-ligand PET/MRI in patients with local and metastatic prostate Cancer. *PLoS One*. 2016;11:e0164392.
9. Noto B, Büther F, Auf der Springe K, et al. Impact of PET acquisition durations on image quality and lesion detectability in whole-body 68Ga-PSMA PET-MRI. *EJNMMI Res*. 2017;7(1):12.
10. Rauscher I, Maurer T, Fendler WP, Sommer WH, Schwaiger M, Eiber M. (68)Ga-PSMA ligand PET/CT in patients with prostate cancer: How we review and report. *Cancer Imaging*. 2016;16(1):14.
11. Afshar-Oromieh A, Wolf M, Haberkorn U, et al. Effects of arm truncation on the appearance of the halo artifact in 68Ga-PSMA-11 (HBED-CC) PET/MRI. *Eur J Nucl Med Mol Imaging*. 2017;44:1636-1646.
12. Heußner T, Mann P, Rank CM, et al. Investigation of the halo-artifact in 68Ga-PSMA-11-PET/MRI. *PLoS One*. 2017;12:e0183329.
13. Watson CC, Newport D, Casey ME, Dekemp RA, Beanlands RS, Schmand M. Evaluation of simulation-based scatter correction for 3-D PET cardiac imaging. *IEEE Trans Nucl Sci*. 1997;44:90-97.
14. Watson CC. New, faster, image-based scatter correction for 3-D PET. *IEEE Trans Nucl Sci*. 2000;47:1587-1594.

15. Watson C, Hayden C, Casey M, Hamill J, Bendriem B. Prompt gamma correction for improved quantification in ^{82}Rb PET. *J Nucl Med*. 2008;49:64P.
16. Hong I, Rothfuss H, Michel C, Casey M. Prompt gamma correction on Ga-68 PSMA PET studies. *IEEE Medical Imaging Conference Record*. 2015;1-2.
17. Watson CC, Hu J, Zhou C. Extension of the SSS PET scatter correction algorithm to include double scatter. *IEEE Nuclear Science Symposium and Medical Imaging Conference*. 2018;1-4.
18. Afshar-Oromieh A, Babich JW, Kratochwil C, et al. The rise of PSMA ligands for diagnosis and therapy of prostate cancer. *J Nucl Med*. 2016;57:79-89.
19. Eiber M, Weirich G, Holzapfel K, et al. Simultaneous ^{68}Ga -PSMA HBED-CC PET/MRI improves the localization of primary prostate cancer. *Eur Urol*. 2016;70:829-836.
20. Schwarzenboeck SM, Rauscher I, Bluemel C, et al. PSMA ligands for PET imaging of prostate cancer. *J Nucl Med*. 2017;58:1545-1552.
21. Lindemann ME, Oehmigen M, Blumhagen JO, Gratz M, Quick HH. MR-based truncation and attenuation correction in integrated PET/MR hybrid imaging using HUGE with continuous table motion. *Med Phys*. 2017;44:4559-4572.
22. Oehmigen M, Lindemann ME, Gratz M, et al. Impact of improved attenuation correction featuring a bone atlas and truncation correction on PET quantification in whole-body PET/MR. *Eur J Nucl Med Mol Imaging*. 2017;45:642-653.
23. Martinez-Möller A, Souvatzoglou M, Delso G, et al. Tissue classification as a potential approach for attenuation correction in whole-body PET/MRI: evaluation with PET/CT data. *J Nucl Med*. 2009;50:520-526.
24. Koesters T, Friedman KP, Fenchel M, et al. Dixon sequence with superimposed model-based bone compartment provides highly accurate PET/MR attenuation correction of the brain. *J Nucl Med*. 2016;57:918-924.
25. Paulus DH, Quick HH, Geppert C, et al. Whole-body PET/MR imaging: quantitative evaluation of a novel model-based MR attenuation correction method including bone. *J Nucl Med*. 2015;56:1061-1066.
26. Blumhagen JO, Ladebeck R, Fenchel M, Scheffler K. MR-based field-of-view extension in MR/PET: B0 homogenization using gradient enhancement (HUGE). *Magn Reson Med*. 2013;70:1047-1057.
27. Blumhagen JO, Braun H, Ladebeck R, et al. Field of view extension and truncation correction for MR-based human attenuation correction in simultaneous MR/PET imaging. *Med Phys*. 2014;41:022303.
28. Lückerrath K, Stuparu AD, Wei L, et al. Detection threshold and reproducibility of ^{68}Ga -PSMA11 PET/CT in a mouse model of prostate cancer. *J Nucl Med*. 2018;59:1392-1397.

29. Eiber M, Herrmann K, Calais J, et al. Prostate cancer molecular imaging standardized evaluation (PROMISE): proposed miTNM classification for the interpretation of PSMA-ligand PET/CT. *J Nucl Med*. 2018;59:469-478.

30. Rowe SP, Pienta KJ, Pomper MG, Gorin MA. Proposal for a structured reporting system for prostate-specific membrane antigen-targeted PET imaging: PSMA-RADS Version 1.0. *J Nucl Med*. 2018;59:479-485.

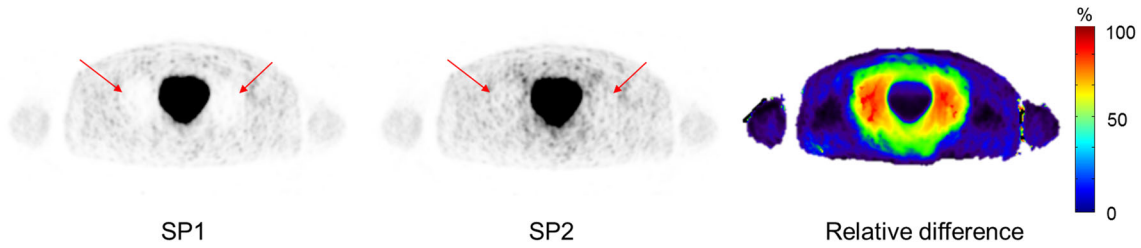


Fig. 1 PET images reconstructed using standard (SP1) and un-renormalized (SP2) scatter correction (SC) and relative difference image between both SC methods. In SP1 corrected PET image a severe halo artifact (grade 4) is observable (red arrows), whereas in SP2 corrected image shows no halo artifact (grade 0) (red arrows). Relative differences in PET activity up to 100 % in this example are maximal in the halo margin; the differences between standard and un-renormalized SC in bladder and surrounding tissue are minor.

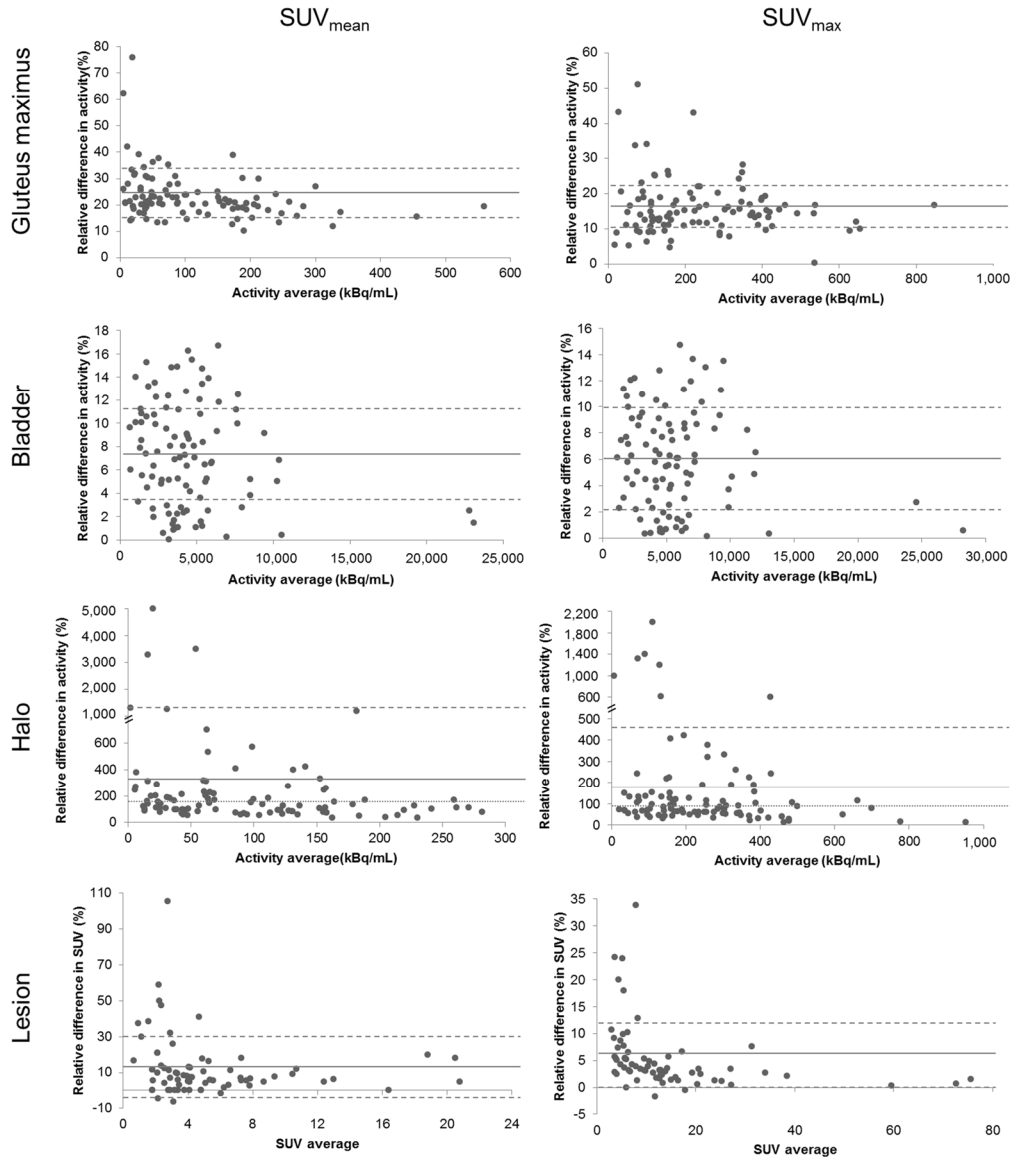


Fig. 2 Bland-Altman plots show the relative difference in measured standardized uptake values (SUV_{mean} , SUV_{max}) in the gluteus maximus, the bladder, the halo margin and in all 74 detected lesions using standard and un-renormalized scatter correction. The solid lines mark the mean value, the dashed lines represent the limits of agreement (standard deviation) and the dotted lines mark the median. Note the overall gain in SUV values due to un-renormalized scatter correction, especially with considerable gain in SUV within the halo margin.

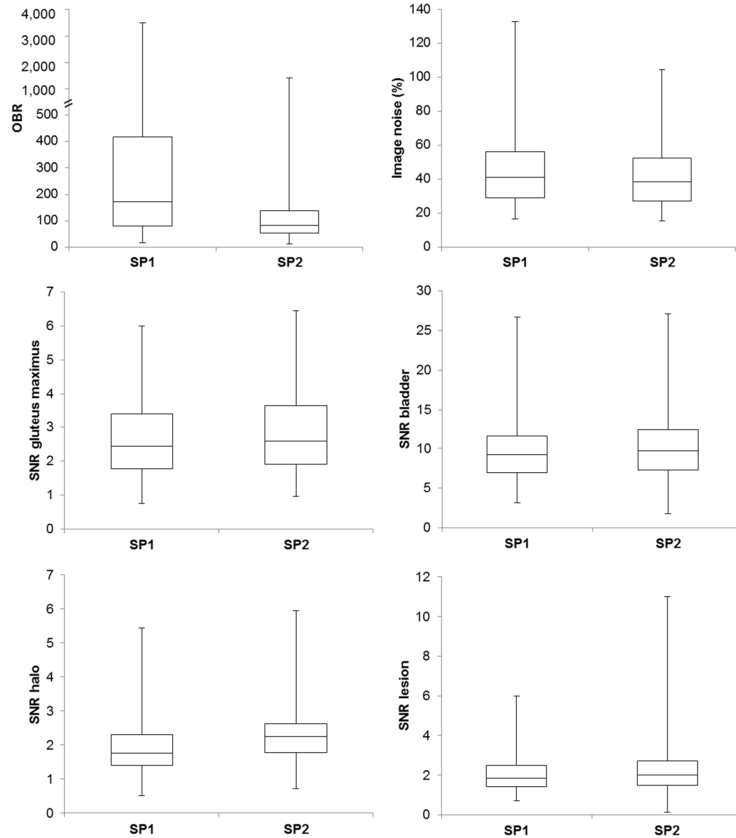


Fig. 3 Boxplots of orbit-to-background-ratio (OBR), image noise and signal-to-noise-ratio (SNR) in the glutemus maximus, the bladder, the halo margin and the n=74 detected lesions using standard scatter correction (SP1) in comparison to un-renormalized scatter correction (SP2). Note that the OBR and image noise decrease with un-renormalized scatter correction, while SNR slightly increases.

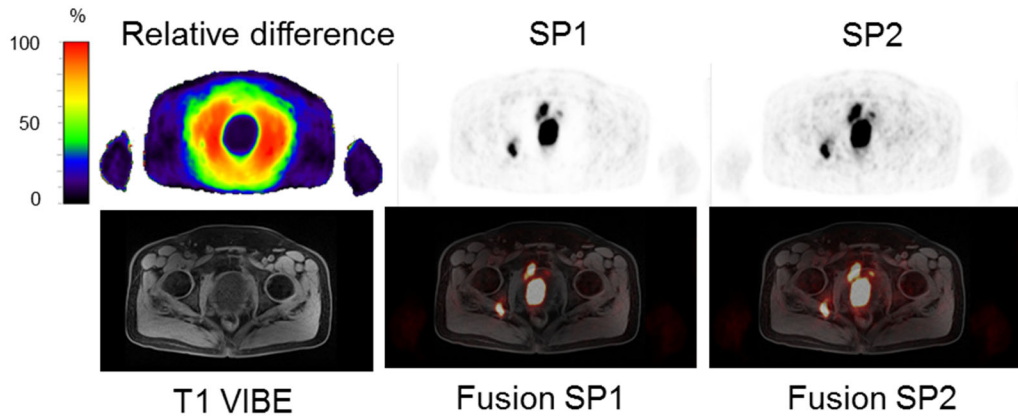


Fig. 4 Patient example with three detected lesions in PET data, an axial T1-weighted VIBE and fusion images with PET data. Relative difference between standard (SP1) and un-renormalized (SP2) scatter correction (SC) show the artifact-reducing impact of un-renormalized SC. Halo artifact was reduced from severe halo presence (grade 4) to no halo artifact (grade 0) using SP2. Relative differences up to 50 % in SUV_{mean} in the lesions were calculated.

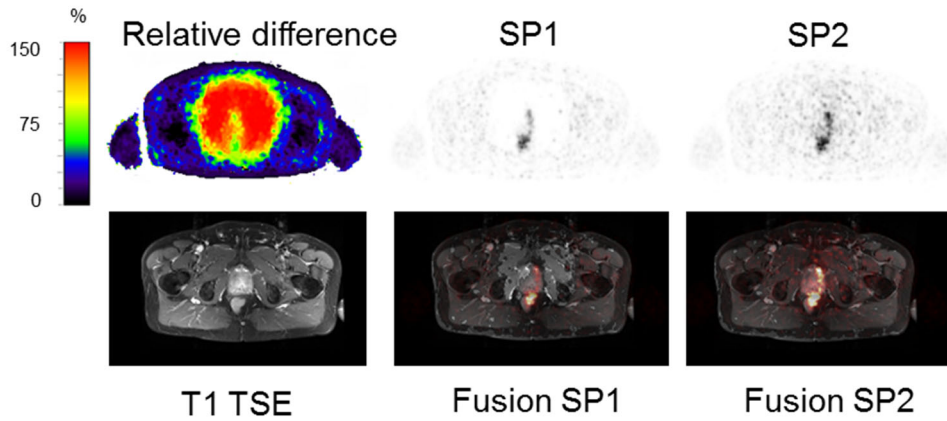


Fig. 5 Patient example with one detected lesion in PET data, an axial T1-weighted TSE and fusion images with PET data. Relative difference between standard (SP1) and un-renormalized (SP2) scatter correction (SC) show the impact of un-renormalized SC. Halo artifact was reduced from strong halo presence (grade 3) to no halo artifact (grade 0) using SP2. A relative difference up to 105 % in SUV_{mean} in the lesion was calculated.

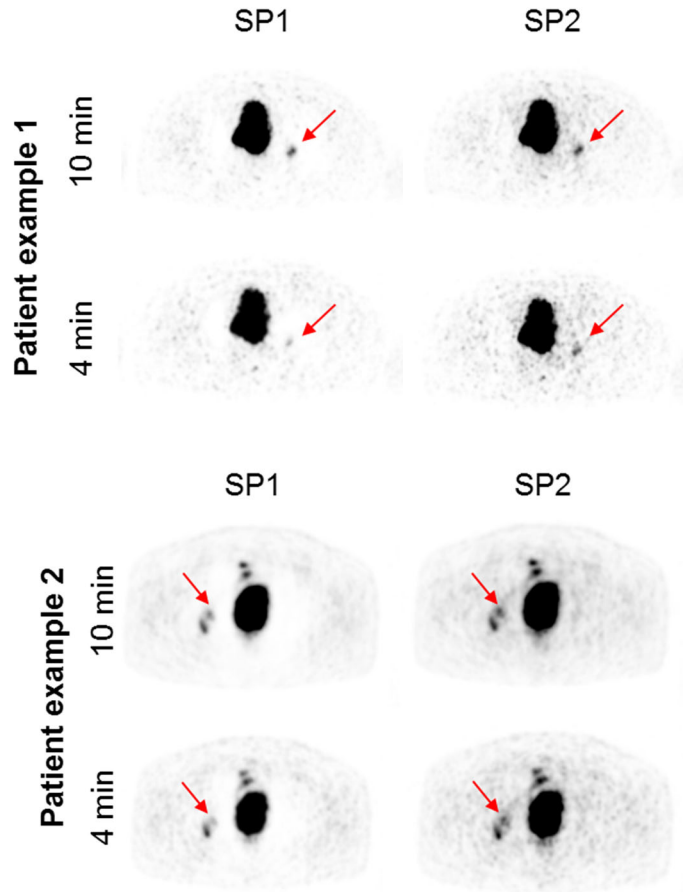


Fig. 6 Evaluation of the impact of PET acquisition time on lesion visibility. Axial PET images of two patient examples with lesions present in the halo artifact margin. For each patient 10 and 4-minute PET time intervals were reconstructed using both standard (SP1) and un-renormalized (SP2) scatter correction (SC). In both time intervals for both patients, the halo artifact was significantly reduced with SP2. While all lesions could be detected in all reconstructions, in the 4-minute time interval the visibility of the marked lesions (red arrow) decreased in the SP1 corrected PET image compared to SP2 corrected data and compared to the 10-minute interval.

halo grade	standard SC (SP1)	improved SC (SP2)
0	n = 1	n = 23
1	n = 31	n = 66
2	n = 39	n = 10
3	n = 26	n = 1
4	n = 3	n = 0

Table 1 The presence of halo artifacts was rated in 5 grades as follows: 0 = no halo artifact, 1 = slight halo presence, 2 = moderate halo presence, 3 = strong halo presence, and 4 = severe halo. n is the number of patients with respective grades. The halo intensity can be reduced by using un-renormalized scatter correction (SC, SP2) over standard SC (SP1).